



Adsorption of metribuzin herbicide on raw maghnite and acid-treated maghnite in aqueous solutions

A. Bettayeb^a, B.A. Reguig^{a,c}, Y. Mouchaal^{b,c,*}, A. Yahiaoui^{a,c}, M.M. Chehimi^d, Y. Berredjem^e

^aLaboratory of Organic, Macromolecular Chemistry and Materials (LCOMM), Route de Mamounia, P.O. Box 763, Mascara, Algeria, email: bettayeb.amel@yahoo.fr (A. Bettayeb), reguigkarim2014@gmail.com (B.A. Reguig), ah_yahiaoui2003@yahoo.fr (A. Yahiaoui)

^bLaboratory of Thin Film Physics and Materials for Electronics (LPCMME), University of Oran1 Ahmed Benbella, 31000 Oran, Algeria, email: mouchaal.younes@gmail.com (Y. Mouchaal)

^cUniversity of Mascara, Faculty of Exact Sciences, Route Mamounira Mascara 29000, Algeria

^dUniversity of Paris East, Icmpe (UMR7182), CNRS, UPEC, F-94320 Thiais, France, email: mmchehimi@gmail.com (M.M. Chehimi)

^eLaboratory of Science and Technology of Water and the Environment, University of Souk-Ahras, Algeria, email: y.berredjem@univ-soukahras.dz (Y. Berredjem)

Received 22 November 2017; Accepted 20 November 2018

ABSTRACT

This study aims to examine the potentialities of raw maghnite and acid-activated maghnite (raw-Mag and Mag-H⁺) for Metribuzin herbicide removal from aqueous solutions. Raw-Mag and Mag-H⁺ were characterized using various analytical techniques such as NMR, BET, FTIR, FRX, ATD and SEM. The effect of various operating parameters such as contact time, Metribuzin concentration, pH, and adsorbent dose were investigated using raw-Mag and H-Mag in batch adsorption system. The results showed that the maximum adsorption capacity was 70.1 and 55.6 mg/g for raw-Mag and Mag-H⁺ respectively at pH 2.5, initial Metribuzin concentration of 20 mg/L, adsorbent raw-M and Mag-H⁺ dosage of 0.5 and 0.2 g/L. The adsorption of Metribuzin herbicide was important in acidic medium for both adsorbents. Furthermore, the adsorption uptake was found to be increased with increase initial concentration. The equilibrium adsorption data were well described by Freundlich and Langmuir isotherms. The kinetic studies showed that the experimental data was best describing by pseudo second order model. The Mag-H⁺ had above 30% adsorption uptake capacity after four regeneration cycles, this was higher than Raw-Mag. It was observed from the values of thermodynamics parameters such as Gibbs free energy (ΔG°), enthalpy (ΔH°), and entropy (ΔS°), that the nature of adsorption is spontaneous.

Keywords: Raw Maghnite, Acid-activated Maghnite, Metribuzin, Adsorption isotherm, Modeling

1. Introduction

Mechanization and modernization of working conditions helped to increase the agricultural production. For many years, intensive agriculture has led to a large scale use of chemicals products, herbicides, fungicides and insecticides in developed countries [1]. In order to improve the quality and productivity of crops, farmers utilize different pesticides to eliminate completely or partially plant para-

sites. Pesticides are a group of dangerous compounds that are capable of polluting water, as they are widely used in agriculture [2,3]. Pollution of groundwater and surface water represents a serious risk to human health due to the potential dangers of their contents in organic and inorganic compounds. The groundwater contaminated with pesticides not only affect the human health when it is directly used for drinking purpose but the food chain is also affected when used for irrigation purposes [4]. Pesticide concentrations in environmental samples are usually low, with tolerance limits around 0.1 $\mu\text{g/L}$ in drinking waters [1]. Contamina-

*Corresponding author.

tion of soil and water by pesticides, particularly herbicides, has drawn the attention of a large number of researchers [5–9]. Metribuzin is a complex macromolecule with formula $C_8H_{14}N_4OS$ and synthetic name (4-amino-6-tert-butyl-4,5-dihydro-3-methylthio-1,2,4-triazine-5 (4H)-one) is one of the most widely used herbicides in the field of agriculture, it belongs to the triazine family of herbicides [10]. It is slightly soluble in water and several organic solvents [11]. Several researchers have applied treatment procedures for elimination of Metribuzin pesticides using various methods, like stripping volt ammetry [12], electrosorption [13], photocatalytic degradation [14] ultraviolet oxidation [15] and adsorption [2,16,17]. Among of these methods still the adsorption is considered as the best method due to its non-specificity and can be used for varieties of contaminants [18]. Recently many studies have been investigated for the development of low-cost adsorbents for Metribuzin removal including natural biosorbents such as coal fly [2] and clay [21].

Maghnite is a compound of montmorillonite clay mineral, -2:1 type aluminosilicate mix. It is highly appreciated for its sorption [22]. Montmorillonite, known as the Maghnite of Maghnia, was used in this study as mineral clay, which was brought from the deposit of Hammam Bouhrara, a small town located in the North Western part of Algeria.

The objective of this research work is to investigate the removal of Metribuzin ($C_8H_{14}N_4OS$) from aqueous solutions using raw montmorillonite and acid-activated montmorillonite (Raw-M and H-Mag). However, to date, no study has ever performed using Maghnite clay to remove Metribuzin pesticide from aqueous solution. Raw and acid-activated maghnite was chosen to eliminate the organic contaminant. In order to understand the adsorption mechanism, it is required to study the adsorption kinetics, mass effect, initial concentration, isotherms, influence of pH on adsorption, and equilibrium models.

2. Materials and methods

2.1. Chemical and reagents

The clay investigated in this work is Montmorillonite named Maghnite, it was obtained from Tlemcen (West Algeria). Metribuzin $C_8H_{14}N_4OS$ (purity: 70%) was provided from Medmac COMPANY. All the other reagents were purchased from Sigma-Aldrich (Chemicals). Bi-distilled water was used in the preparation of the pesticide solutions. The chemical structure of the ($C_8H_{14}N_4OS$) is given in Fig. 1.

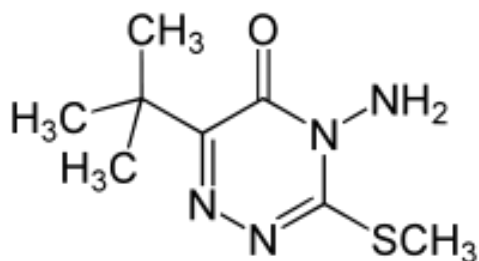


Fig. 1. Chemical structure of metribuzin.

2.2. Preparation of clay adsorbent

The sample of mineral clay (maghnite of Maghnia) was washed with distilled water to remove impurities. Next, 50 g of clay was dispersed into one liter of distilled water. The solution obtained was maintained under magnetic stirring, at a speed of 250 rpm for 24 h at room temperature 298 K. After, the supernatant part was filtered and dried in the open air. Afterward, the resulting product was ground for 30 min using a Prolabo ceramic balls grinder, and sieved. Then, it was dried at 423K for 2 h, and stored in glass vials, hermetically sealed, for later use.

Montmorillonite (Mag-H⁺) was prepared according to the procedure in previous studies [23]. Amount of montmorillonite (10 g) obtained after sedimentation, was dispersed into 250 mL of HCl (0.1 M). Then, the mixture was put under magnetic stirring at room temperature, for 4 h. Montmorillonite was filtered by centrifugation, at the speed of 3500 rpm, and then washed with bi-distilled water until total removal of chlorides (Cl⁻). Montmorillonite was dried and ground. A quantity of 10 g of the montmorillonite obtained was dispersed into 500 mL of peroxide (H₂O₂) to 10 volumes, and was kept under magnetic stirring at 250 rpm for 24 h. The mixture obtained was heated at 70°C for 30 min, filtered by centrifugation at 3500 rpm and washed with bi-distilled water. Finally, the Montmorillonite was dried and stored in hermetically sealed glass vials for later use.

2.3. Characterization of the clay adsorbent

The samples were characterized by BET, XRF, XRD, NMR, SEM and DTA techniques. The specific surface areas of the material were measured by Brunauer-Emmett-Teller (BET) method [24,25], while the adsorption of gases (N₂ at 77 K and CO₂ at 273 K) was used for assessing the narrower micropores (VDR (CO₂)) (pore size less than 0.7 nm) and also by applying the Dubinin-Radushkevich equation to the ratio of pressures lower than 0.025 [25]. The measurements were carried out using a volumetric nitrogen adsorption device, of automated Quantachrome type. The samples were processed in the temperature range from 195 to 949°C, for 24 h. The adsorption and desorption processes were followed by measuring the variation of the thermal conductivity of a gas stream composed of 99.99% nitrogen (adsorbate) and 70% helium at 99.99% (carrier gas). The specific surface area of a solid is given by :

$$S_{\text{BET}} = \frac{\sigma \times V_s \times N}{V_m} \quad (1)$$

where σ is the surface occupied by an adsorbate molecule, it is equal to 16.2 \AA^2 for nitrogen, at 77 K. N is Avogadro's number (6.023×10^{23} molecules), V_m the molar volume (22.4 L), and V_s the volume of adsorbed vapor per gram of solid, at pressure P .

X-ray diffraction measurements were performed on a Bruker CCD-Apex apparatus, diffractometer with copper $K\alpha$ radiation ($\lambda = 1.54 \text{ \AA}$), generator setting of 40 kV and 40 mA, a scanning speed of $0.01^\circ \text{ min}^{-1}$ and a scanning region of $3\text{--}70^\circ$. The d_{001} spacing of maghnite particles was calculated according to Bragg's law ($d = \lambda / 2\sin\theta$).

X-ray fluorescence (XRF) was carried out using the PW 1480 Philips device, with UNIQANT II software, in order

to determine the concentrations of elements in a semi-quantitative manner. NMR spectra of ^{27}Al in the samples of Raw-Mg and Mag- H^+ were recorded on a Bruker 500 ASX spectrometer at 59.6 and 130.3 MHz, respectively. The spinning frequency used was 11.5 KHz.

Scanning electron microscopy (SEM) was used for determination of the raw maghnite and acid-activated maghnite morphological structure before and after adsorption. The apparatus used is a scanning electron microscope, of HITACHI SC-2500 model, which operates at a voltage of 200 kV.

Thermodynamic analysis in a range of temperature 25–900°C by 10°C min^{-1} under the protection of nitrogen on a DTA instrument.

2.4. Batch adsorption experiment

The adsorption spectrum of Metribuzin (Fig. 2) reveals the existence of an absorption band which corresponds to $\lambda = 293$ nm. Sorption equilibrium experiments were carried out by adding a fixed amount of raw-Mag (M_1) and Mag- H^+ (M_2) into a sealed glass flasks containing a definite volume (200 mL) of different initial concentration (10–50 mg/L) without changing their pH. The temperature was maintained constant. The initial concentration of Metribuzin solution was 20 mg/L for all experiments, except for those carried out to examine the effect of initial concentration. The experiments were investigated at well-defined temperature, stirring speed (250 rpm) was applied (Heidolph motor stirrer) for t minutes until equilibrium (that this the moment when no more Metribuzin is removed by adsorbents) was achieved. The initial pH values (pHi) for solutions were adjusted in the range 1–12 by adding minimum amounts of 0.1 N NaOH or 0.1 N HCl. Samples of solutions were analyzed for the remaining Metribuzin concentration with a UV-Vis spectrophotometer.

The amount of Metribuzin adsorbed per unit mass of raw maghnite and acid-activated maghnite was calculated, using the following equation:

$$q_t = \frac{(C_0 - C_t)V}{W} \quad (2)$$

where C_0 is and the initial concentration ($\text{mg}\cdot\text{L}^{-1}$), C_t is the concentration of organic pollutants at time t (mg/L), V is

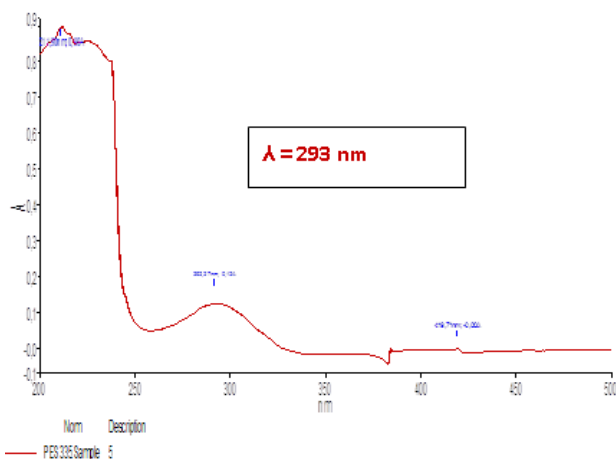


Fig. 2. Wave length of metribuzin, $C_0 = 50$ mg/L.

the volume of solution used (mL), and W is the weight of the adsorbent (g).

3. Results and discussion

3.1. NMR

The NMR spectra of ^{27}Al in both samples, i.e. raw maghnite and acid-activated maghnite (Fig. 3), reveal the existence of aluminum in both tetrahedral environments, with resonances centered on 60 and 68 ppm. Similar results have been obtained in other studies [26].

The NMR spectra of ^{29}Si for raw maghnite and acid activated maghnite are shown in Fig. 4. The dominant resonance at -93.5 ppm corresponds to Q3 (OAl) units, i.e. SiO_4

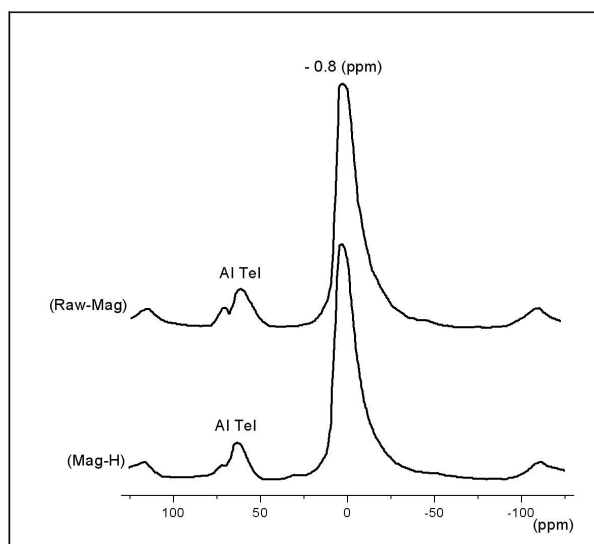


Fig. 3. ^{27}Al MAS NMR spectra of raw-maghnite and maghnite- H^+ .

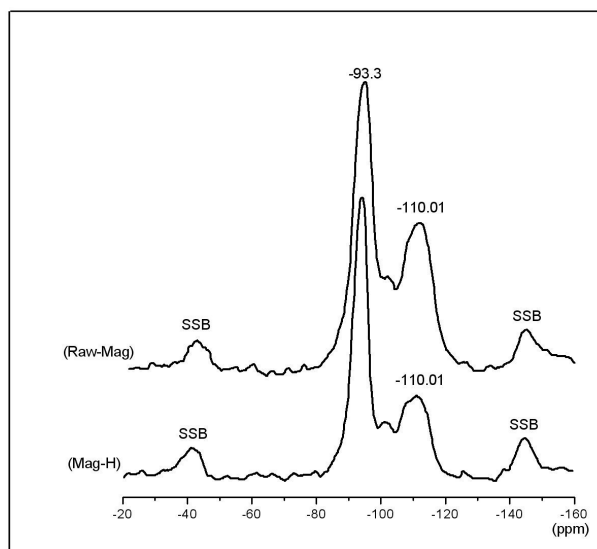


Fig. 4. ^{29}Si MAS NMR spectra of raw-maghnite and maghnite- H^+ .

groups cross linked in the tetrahedral sheets with no aluminum in the neighboring tetrahedral [27]. The resonance at -110.01 ppm corresponds to three-dimensional (3D) silica with no aluminum, it is designated as Q4 (OA1).

3.2. Textural properties

The specific surface area of powder is estimated from the amount of nitrogen adsorbed in relation to its pressure at the boiling temperature of liquid nitrogen, and at normal atmospheric pressure. The results are presented in Table 1. It can be noted that the specific surface area achieves $140 \text{ m}^2\cdot\text{g}^{-1}$ for raw maghnite and $161 \text{ m}^2\cdot\text{g}^{-1}$ for acid-activated maghnite.

The acid activation increases the number of active sites of the adsorbent [28], which facilitates the penetration of Metribuzin molecules and their accessibility in the porous structure of the clay.

3.3. X-ray diffraction analysis

The X-ray diffraction method is particularly suitable for studying the structure of maghnite. In the XRD spectra of clays, the more intense lines correspond to the reflections that are perpendicular to the planes of sheets; they are representative of the reticular distances d_{001} . These distances allow, after subtraction of the thicknesses of the sheets, to deduce the inter-sheet distances. To validate the intercalation of H^+ ions between the clay layers (montmorillonite), a XRD analysis of raw and acid-activated clay was performed. The results of this analysis are displayed in the diffractogram of Fig. 5. The X-ray diffraction analysis of acid-activated maghnite, as compared to raw maghnite (Table 2), shows that the interlayer distance d_{001} (\AA) decreases. The X-ray diffraction spectra (Fig. 5) are in agreement with the literature [29]. The presence of a major amount of montmorillonite is shown by the appearance of a series of intense peaks and the presence of other crystalline phases such as Quartz, Feldspar and calcite was detected (Table 3).

3.4. Fourier transform infrared spectroscopy analysis

The two spectra were superimposed in order to be compared (Fig. 6). This figure reveals that the two FTIR spectra of acid-activated maghnite and raw maghnite are super imposable, which means that there is a juxtaposition of all the bands related to the vibrations of the OH groups, the bands of angular deformation due to absorbed water molecules, as well as the peak attributed to Si-O-Al elongations. The effects of acid activation on the FTIR spectrum of acid-activated maghnite (Fig. 6) are summarized as follows:

On acid treatment, the intensity of the absorption band at 3630 cm^{-1} (AlAlOH) coupled by AlMgOH stretching vibrations decreases. The bands at 3425 cm^{-1} and 3200 cm^{-1} (water absorption between layers) become more diffuse with acid treatment.

The intensity of the Si-O stretching band and Si-O-Si stretching bands at 1116 , 1043 and 998 cm^{-1} have not been affected by acid treatment. With acid treatment, the AlAlOH (920 cm^{-1}), $\text{AlFe}^{3+}\text{OH}$ (883 cm^{-1}) and AlMgOH (846 cm^{-1}) deformation bands decrease. The intensity of

Table 1
Textural characterization of Mag- H^+ , and raw-mag

Samples	$S_{\text{B.E.T}}$ ($\text{m}^2\cdot\text{g}^{-1}$)
Raw-M	140
Mag- H^+	161

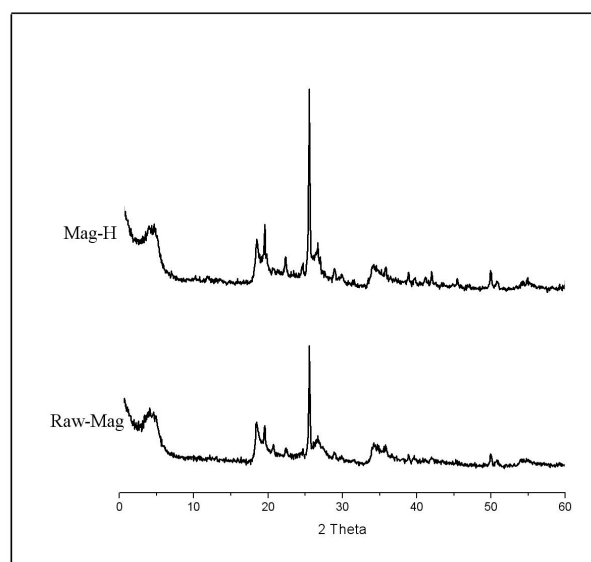


Fig. 5. X-ray diffraction of untreated clay (Raw-Mag) and acid treated clay (Mag- H^+).

Table 2
Values of interfoliar distances d_{001} of raw-M and maghnite- H^+

Sample	2θ ($^\circ$)	d_{001} (\AA)
Raw-M	6.94	12.71
Mag- H^+	6.59	11.76

the band at 796 cm^{-1} increases with acid treatment, and this reveals the alterations in the amount of amorphous silica; this result is in good agreement with the findings of other researchers [30]. The intensity of the band at 628 cm^{-1} (either Al-OH or Si-O bending and/or Al-O stretching vibration) gradually decreases with acid treatment, which is also in line with the findings of Komadel [31]. The intensity of the band (Si-O-Al and Si-O-Mg coupled with an OH vibration and Si-O bending vibration) at 467 cm^{-1} remains essentially unchanged.

The major phase (montmorillonite) represents about 75% of raw material in weight, and the main impurities are quartz, feldspar, carbonates and cristobalite as well as some organic matter.

3.5. X-ray fluorescence

The chemical composition of both adsorbents (raw maghnite and acid maghnite) is defined using the results obtained from the XRF analysis; they are given in Table 4. The results relative to X-ray fluorescence analysis, indicate

Table 3
XRD characteristic of raw-maghnite and maghnite-H⁺

M-X	D _{hkl} (Å)	hkl	Nature of sample
Raw-Maghnite	12.50	001	Montmorillonite
	4.47	110	Montmorillonite
	4.16	110	Quartz
	3.35	110	Quartz
	3.21	110	Feldspath
	3.03	100	Calcite
	2.55	200	Montmorillonite
	1.68	009	Montmorillonite
	1.49	060	Montmorillonite
	Maghnite-H ⁺	15.02	001
4.47		110	Montmorillonite
4.16		110	Quartz
3.35		110	duartz
3.21		110	Feldspath
3.03		110	Calcite
2.55		200	Montmorillonite
1.68		009	Montmorillonite
1.49		060	Montmorillonite

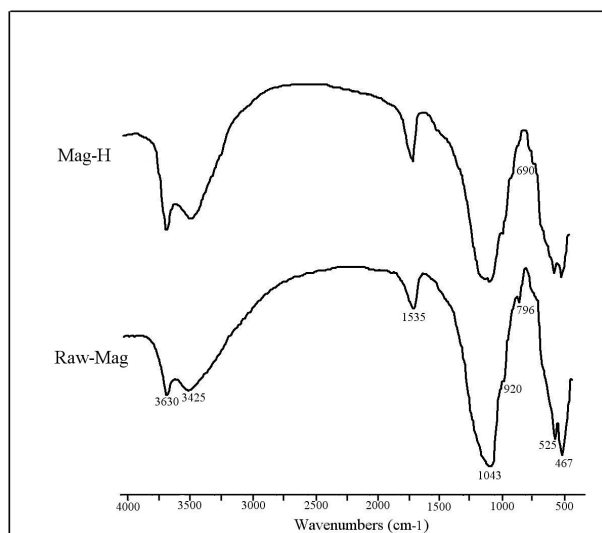


Fig. 6. FTIR spectra of untreated clay (raw-mag) and acid treated clay (Mag-H⁺).

that the sample contains a very small amount of Fe₂O₃ (1.16%); it is saturated with silicon (SiO₂) at more than 69%, and is associated to cations Na⁺ and H⁺. The space between the sheets of sodium montmorillonite contains SiO₂ and Al₂O₃ at 14.67%. Substituting and then decreasing the content in oxide (Fe₂O₃, CaO, MgO, TiO₂, ZnO, MnO, and SO₃) leads to the total disappearance of the elements (SrO, Y₂O₃, ZnO, Na₂O). The ratio SiO₂/Al₂O₃ was found to be equal to 4.75. These are silico-aluminous materials where SiO₂ is predominant. The similar results are found by Zeggai et al. [32].

Table 4
Composition (in weight percent) of raw-montmorillonite (raw-M) and acidic montmorillonite (Mag-H⁺)

Composition	Raw-M	Mag-H ⁺
Na ₂ O	0.50	0.21
MgO	1.07	0.80
Al ₂ O ₃	14.67	14.03
SiO ₂	69.71	71.7
P ₂ O ₅	0.013	0.012
SO ₃	0.91	0.34
K ₂ O	0.79	0.77
CaO	0.30	0.28
TiO ₂	0.177	0.15
MnO	0.098	–
Fe ₂ O ₃	1.16	0.71
PF	11	11

3.6. Differential thermal analysis

Differential thermal analysis (DTA) was used as a thermal analysis, to identify and test the purity of the product obtained. Fig. 7 shows the DTA thermogram of the Raw-Mag and Mg-H⁺ from 25 to 900°C. The raw-maghnite sample showed an endothermic peak at 100°C, due to the loss of adsorbed water. Also, it was seen two endothermic peaks, at 200°C and 635°C, the former could be due to the dehydration of hydrous impurities and the later due to the dehydroxylation of the clay layers [33]. However on acid treatment, it was showed four endothermic peaks, at 65.4, 180, 425 and 650°C.

3.7. Scanning electron microscopy

Scanning electron microscope images of untreated clay (Raw-Mag) and acid treated clay (Mag-H⁺) are shown in Fig. 8. The micrographs confirm that the material is forming micron size agglomerates for distance more than 20 μm. Compared with modified montmorillonite, the raw montmorillonite's particles were larger and its sheets were also thicker. Activated montmorillonite's surface was relatively tight [34], it was greatly changed. The pore spaces were become narrow. This indicates that the modification expanded the interlayer space and formed a disordered intercalated structure, which is in agreement with the results of XRD patterns [35].

4. Adsorption studies

The adsorption process of metribuzin on raw and acid-activated clays has been discussed with respect to different factors.

4.1. Effect of mass

Fig. 9 shows the influence of varying the mass of the adsorbent (maghnite) on the adsorption of metribuzin. It is noted that the increase in the quantity of adsorbent, results

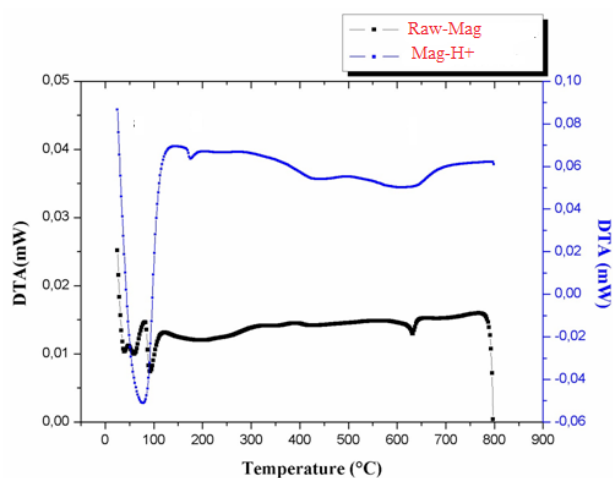
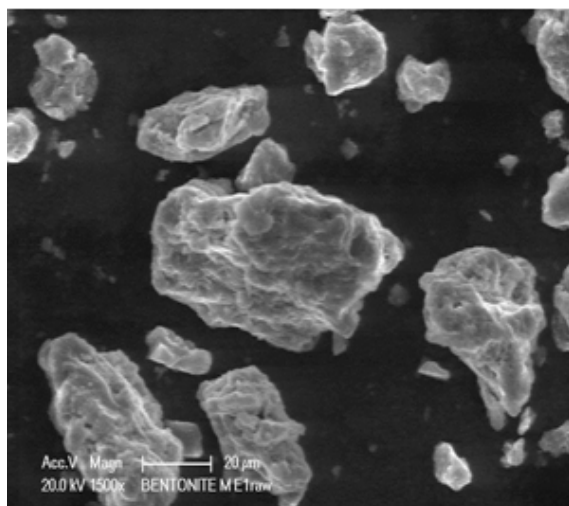
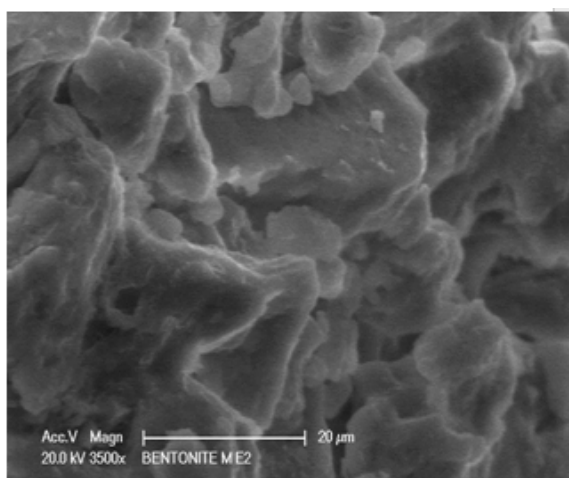


Fig. 7. DTA curves of Raw-Mag and H-Mag-H⁺ up to 900°C, at heating rate of 10°C min⁻¹.



(a)



(b)

Fig. 8. SEM images of Raw-Mag (a) and Mag-H⁺ (b).

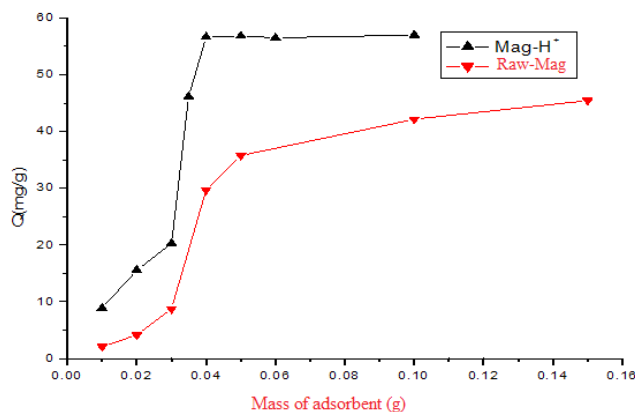


Fig. 9. Effect of the mass montmorillonites (Mag-H⁺ and Raw-Mag) on adsorption metribuzin. ($C_i = 20 \text{ mg L}^{-1}$, $T = 20^\circ\text{C}$, stirring speed = 250 rpm, and $\text{pH} = 2.5$).

in an improvement in the retention efficiency up to the maximum point.

The above mentioned results may be attributed to the increase in the usable area due to the large quantities of adsorbent. In fact, if the mass of the solid in the solution is large, the number of adsorption sites will also be important. Therefore, the probability of molecule-site encounter also increases, leading to better retention. It can be seen that good yields are obtained in the case of acid-activated maghnite for masses equal to 0.040 and 0.10 g of raw and acid maghnite, respectively, the maximum amount of metribuzin adsorbed can reach the value of 65 and 40 mg/g for Mag-H⁺ and raw-Mag respectively.

4.2. Effect of stirring time

The influence of contact time on metribuzin removal by 0.04 g and 0.1g of raw-Mag and Mag-H⁺ at pH 2.5 and 20°C with an initial metribuzin concentration 20mg/L are shown in Fig. 10. It was seen that the efficiency of Metribuzin removal increases with the stirring time. The maximum values of Metribuzin elimination was found about 55 and 70 mg/g, for raw-Mag and acid treated maghnite respectively. Two steps can be distinguished in the adsorption kinetics: In the first, a fast adsorption within a few minutes to followed by a gradual process of around 2 h and 3 h for raw-Mag and Mag-H⁺ respectively until the equilibrium was established. This two-step adsorption process has been previously reported by Chen et al. [36], where the initial fast process of sorption is a surface phenomenon, then slow migration and diffusion of the compound. A comparison with other published data shows that the equilibrium time reported is much shorter than others. Kitous et al. [13] were found that the adsorption of metribuzin pesticide was completed in 13 h. However, Chen et al. [36] demonstrated that phorate and terbufos adsorption were reached an equilibrium after 6 h at pH 5.7 and 8.7.

4.3. Effect of initial concentration

Fig. 11 shows the sorption uptake vs, the initial metribuzin concentration at 20°C. It was observed that the

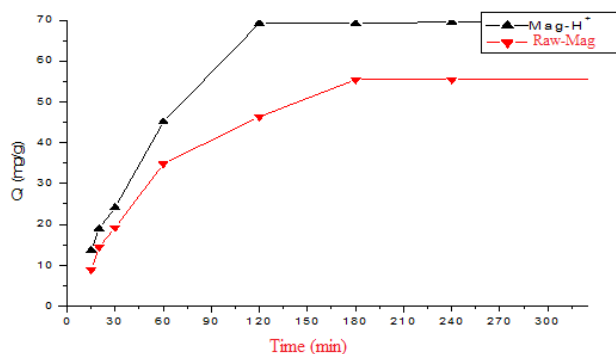


Fig. 10. Effect of contact time on the adsorption of metribuzin to Raw-Mag and Mag-H⁺. ($C_i = 20 \text{ mg L}^{-1}$, $T = 20^\circ\text{C}$, stirring speed = 250 rpm, and $\text{pH} = 2.5$).

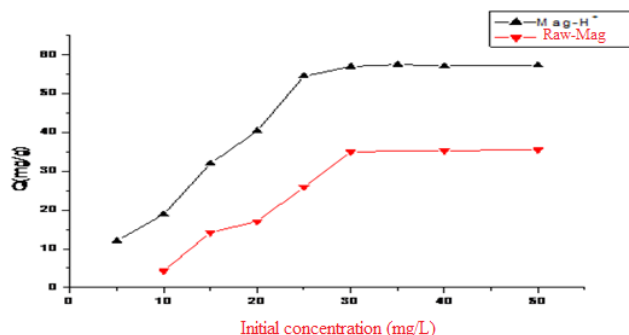


Fig. 11. The isotherms of Metribuzin adsorption from aqueous solutions on the Raw-Mag and Mag-H⁺ ($T = 20^\circ\text{C}$, Stirring speed = 250 rpm, and $\text{pH} = 2.5$).

adsorption of metribuzin increased with increasing initial pesticide concentration, the amount of pesticide removed at equilibrium increased from 0.4 to 30 mg/g and 12.5 to 60 mg/g for raw-Mag and Mag-H⁺ respectively, this is in good agreement with the increase in the surface area. The Acid-treated maghnite displays a higher adsorption curve than that of raw maghnite. The adsorption isotherms on both types of maghnite have an L-type profile. This isothermal profile suggests that adsorption is driven by the affinity between Metribuzine molecules ($\text{C}_8\text{H}_{14}\text{N}_4\text{O}_5$) and the hydrophobic intercalary layer [37] due to the intercalation of acid-activated maghnite.

4.4. Effect of pH solution

Fig. 12 shows the effect of initial pH on the adsorption of metribuzin by raw-Mag and Mag-H⁺. The pH of the solution plays an important role in the adsorption of pesticides onto the surface of the adsorbent [38]. The effect of pH on metribuzin adsorption was examined at pH values from 1 to 12 and was evaluated. It can be seen that the adsorption onto acid-activated maghnite and raw maghnite increased slowly with increasing pH to reach a maximum values, at pH 2.1 and 3.8 for Mag-H⁺ and raw-Mag respectively.

The structure of maghnite consists of negatively charged hydroxide sheets [22]. At higher pH values, the surface of maghnite becomes negatively charged and electrostatic

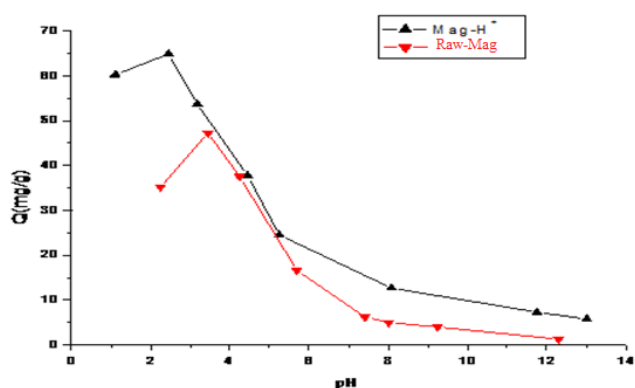


Fig. 12. Effect of pH on metribuzin adsorption on the Mag-H⁺ and Raw-Mag. ($T = 20^\circ\text{C}$, $M_1 = 0.1 \text{ g}$, $M_2 = 0.04 \text{ g}$, $C_i = 20 \text{ mg L}^{-1}$, and stirring speed = 250 rpm).

repulsion between the adsorbent surface and anions of metribuzin become significantly, therefore, the adsorption efficiency of metribuzin decreases.

5. Adsorption isotherm studies

The adsorption isotherm is the curve that relates, at a fixed temperature, the quantity of product adsorbed on the initial mass of the adsorbent, to the concentration in the remaining fluid phase. It is used to determine the maximum adsorption capacity of adsorbates on the adsorbents, in mg/g or mmol/g. To exploit the data on the adsorption isotherm of metribuzin by raw maghnite and acid-activated maghnite, at various temperatures, the following Langmuir [Eq. (3)] and Freundlich [Eq. (4)] equations were used in their linear form [39].

The Langmuir adsorption model is based on the assumption that maximum adsorption corresponds to a saturated monolayer of solute molecules on the adsorbent surface [40].

$$\frac{C_e}{q_e} = \frac{1}{K_L q_m} + \frac{1}{q_m C_e} \quad (3)$$

where K_L is the thermodynamic equilibrium constant of Langmuir ($\text{L}\cdot\text{mg}^{-1}$), q_m the maximum adsorption capacity per unit mass of the adsorbent ($\text{mg}\cdot\text{g}^{-1}$), q_e the adsorption capacity per unit mass of the adsorbent ($\text{mg}\cdot\text{g}^{-1}$) at equilibrium, and C_e the concentration of adsorbate at equilibrium ($\text{mg}\cdot\text{L}^{-1}$).

The Freundlich model is based on an empirical relationship between the adsorption and adsorbate concentration it is employed to describe heterogeneous systems and reversible adsorption and is not restricted to monolayer formation [41].

$$\ln q_e = \ln K_f + \frac{1}{n} \ln C_e \quad (4)$$

where q_e is the amount adsorbed ($\text{mg}\cdot\text{g}^{-1}$), C_e the equilibrium concentration of the adsorbate ($\text{mg}\cdot\text{g}^{-1}$), K_f is a constant indicative of the relative sorption capacity of the sorbent ($\text{mg}^{-1-\frac{1}{n}} \text{L}^{\frac{1}{n}} \text{g}^{-1}$) and n are the constants that char-

acterize the Freundlich system, and which correspond to the adsorption capacity and adsorption force, respectively.

The equilibrium parameters obtained with the Freundlich and Langmuir representations are reported in Table 5. The values of the correlation coefficient are higher for the Langmuir isotherm than for the Freundlich isotherm, and this means that the Langmuir isotherm equation better represents the adsorption process of Metribuzin by raw maghnite and acid-activated maghnite. This is probably due to the uniform distribution of active sites on the surface of maghnite. The maximum adsorption capacity (q_m) of Langmuir increases from 57.12 to 72.18 $\text{mg}\cdot\text{g}^{-1}$ for raw maghnite and acid-activated maghnite, when the temperature rises from 20 to 50 °C.

The thermodynamic constant of adsorption equilibrium (K_L) decreases from 0.89 to 0.45 $\text{L}\cdot\text{g}^{-1}$ as the temperature increases within the interval under consideration. The dimensionless factor (R_L) is calculated by the following equation:

$$R_L = \frac{1}{1 + K_L C_0} \quad (5)$$

where C_0 (mg/L) is the initial concentration of the adsorbate, and K_L ($\text{L}\cdot\text{g}^{-1}$) is the Langmuir constant.

The R_L parameter shows whether the adsorption system is favorable if ($0 < R_L < 1$), unfavorable ($R_L > 1$), irreversible ($R_L = 0$) or linear ($R_L = 1$) [42].

This coefficient indicates that the adsorption process becomes effective when it takes values between 0 and 1 ($0 < R_L < 1$). The values of R_L from 0.043 to 0.068, for the various temperatures considered, indicate that metribuzin is actually adsorbed by raw maghnite and acid-activated maghnite and the Langmuir isotherm is favorable. These results are consistent with those obtained in previous works by [43,44].

The efficiency of raw maghnite and acid-activated maghnite is even higher than the coefficient of intensity $1-n < 1$, indicating that the adsorption is favorable and where $1/n$ above one is an indicative of cooperative adsorption [45].

6. Adsorption kinetics

The kinetic data for metribuzin herbicide adsorbed onto raw maghnite and acid-treated maghnite were computed by pseudo first order [46] [Eq. (6)] and pseudo-second order [47] [Eq. (7)]. These models are catalog as beneath:

Table 5

Freundlich and Langmuir coefficients obtained from the adsorption isotherms of metribuzin on the Raw-M and the Mag-H⁺ at 298 K and pH 2.5

Sample	Langmuir constant			Freundlich constant		
	q_m (mg/g)	K_L (l/g)	R^2	n	K_f	R^2
Mag-H ⁺	72.18	0.89	0.99	2.18	3.02	0.95
Raw-Mag	57.12	0.45	0.97	1.97	2.34	0.96

$$\ln(q_e - q_t) = \ln q_e - k_1 t \quad (6)$$

where q_e and q_t are the quantities of metribuzin ($\text{mg}\cdot\text{g}^{-1}$) adsorbed at equilibrium and at time t (min) respectively, and k_1 is the rate constant (min^{-1}).

$$\frac{1}{q_t} = \frac{1}{k_2 q_e^2} + \frac{t}{q_e} \quad (7)$$

From the graphic representation of the variation of $\ln(q_e - q_t)$ as a function of t , it is possible to determine k_1 and q_e .

Table 6 summarizes the values of the kinetic parameters of the first-order Lagergren equation, namely the correlation coefficient (R^2), rate constant (k_1), adsorption calculated at equilibrium q_e (cal) and experimental adsorption at equilibrium q_e (exp). These results show that the correlation coefficient (R^2) assumes the highest value (0.9462) at the temperature of 20 °C. The values of q_e (exp) increase with the temperature while those of q_e (cal) decrease. The negative evolution of q_e (cal) as a function of temperature proves that the first-order equation is not adequate to have a good kinetics of Metribuzin adsorption by maghnite.

The values of k_2 and q_e were calculated from the origin and slope of the graphical representation of the variation of t/q_t as a function of t . Table 6 presents the values of k_2 , R^2 , q_e (cal) and q_e (exp) as a function of temperature. These results show that the correlation coefficient (R^2) has values greater than 0.98 and that the values of q_e (cal) are comparable to those of q_e (exp), for any temperature in the considered range. This confirms that the sorption kinetics of Metribuzin by raw and acid-activated maghnite follows a second order reversible sorption rate law. In the second order equation of adsorption kinetics, it is assumed that the phase limiting adsorption is chemisorption, which involves forces and electron exchanges between the adsorbent and the adsorbate [48].

Also, it can be noted that the second-order model corresponds better to the experimental data for all the Metribuzin concentrations used (between 20 and 50 $\text{mg}\cdot\text{L}^{-1}$). The second-order model is based on the assumption that the rate limiting step can be chemical adsorption, involving valence forces by sharing or exchanging electrons between the adsorbent and the adsorbate [49].

7. Thermodynamic evaluation of the adsorption process

The adsorption capacity of metribuzin by raw maghnite and acid-activated maghnite was studied in the temperature range from 293 to 323K. The free energy of adsorption (ΔG°) and the entropy (ΔS°), and enthalpy changes (ΔH°) in the adsorption process are related by the Van't Hoff equations [50]:

$$\Delta G^\circ = -RT \ln K_0 \quad (8)$$

$$\Delta G^\circ = \Delta H^\circ - T\Delta S^\circ \quad (9)$$

$$K_L \frac{q_e}{C_e} \quad (10)$$

Table 6

Comparison of the first- and second-order adsorption rate constants, for calculated ($q_{e(cal)}$) and experimental ($q_{e(exp)}$) values at metribuzin of concentration 30 mg L⁻¹ and pH 2.5

Adsorbent	$q_{e(exp)}$ (mg/g)	First-order kinetic model			Second-order kinetic model		
		$q_{e(cal)}$ (mg/g)	k_1 (min ⁻¹)	R ²	$q_{e(cal)}$ (mg/g)	k_2 (min ⁻¹)	R ²
H-Mag	70.1	82.4	0.017	0.94	74.9	0.007	0.98
Raw-Mag	55.6	62.9	0.014	0.93	64.5	0.0067	0.97

Table 7

Thermodynamic constants for the adsorption of Metribuzin on raw-M, H-M montmorillonites at various temperatures

Thermodynamic parameters	ΔH° (kJ/mol)	ΔS° (J/mol)		ΔG° 293 (kJ/mol)		ΔG° 303 (kJ/mol)		ΔG° 313 (kJ/mol)		ΔG° 323 (kJ/mol)		
		H-M	raw-M	H-M	raw-M	H-M	raw-M	H-M	raw-M	H-M	raw-M	
C_i (ppm)	H-M	raw-M	H-M	raw-M	H-M	raw-M	H-M	raw-M	H-M	raw-M	H-M	raw-M
20	2.16	0.53	33.67	28.58	-9.86	-8.37	-10.20	-8.66	-10.54	-8.94	-10.87	-9.23
30	6.09	0.65	25.80	28.10	-7.55	-8.23	-7.81	-8.51	-8.07	-8.79	-8.33	-9.08
40	18.00	1.79	29.74	35.14	-8.70	-10.29	-8.99	-10.64	-9.29	-11.00	-9.59	-11.35
50	2.01	0.34	32.76	25.76	-9.60	-7.55	-9.93	-7.80	-10.25	-8.06	-10.58	-8.32

where T is the temperature (K), R is the gas constant (8.314 J·mol⁻¹·K⁻¹), ΔH° is the standard enthalpy (kJ·mol⁻¹), the standard entropy (kJ·mol⁻¹·K⁻¹), and K_0 the sorption distribution coefficient (L·g⁻¹).

The sorption distribution coefficient K_0 can be expressed in terms of enthalpy, entropy and temperature, as shown in Eq. (11) below:

$$\ln K_0 = \frac{\Delta S^\circ}{R} - \frac{\Delta H^\circ}{RT} \quad (11)$$

The thermodynamic parameters of the adsorption isotherm are listed in Table 7. They have been used to explain the mechanism of the adsorption process of Metribuzin herbicide by raw and acid-activated maghnite. The values demonstrate non spontaneous and favorable sorption process. The positive values of heat of reaction ΔH° indicated that the sorption is endothermic [51]. On the other hand, the negative values of the change in free energy depict the spontaneous nature of the process. Finally, negative of ΔS° are very large and correspond to a decrease in the degree of freedom of the sorbed species

8. Desorption and regeneration

The results of regeneration study are presented in Fig. 15. Desorption experiments were performed using distilled water. The Mag-H⁺ showed higher resilience than Raw-Mag after four regeneration cycles, it had above 30% adsorption uptake capacity after four regeneration cycles. The desorption efficiency may have been enhanced by repulsion activities between the metribuzin molecules and protonation of the Acid treated clay surface. The decrease in the adsorption uptake of metribuzin on Mag-H⁺ with increasing regeneration cycles was attributed to the increase in the adsorbate molecules that were strongly attached to the surface of the adsorbent via chemical adsorption.

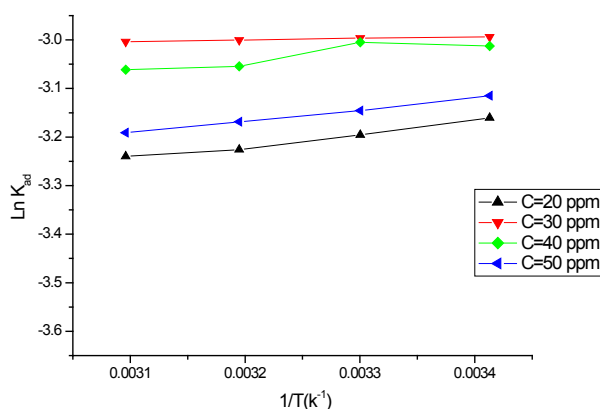


Fig. 13. Linearization curves of the distribution constant ($\ln K_0$) as a function of temperature ($1/T$) for Mag-H⁺.

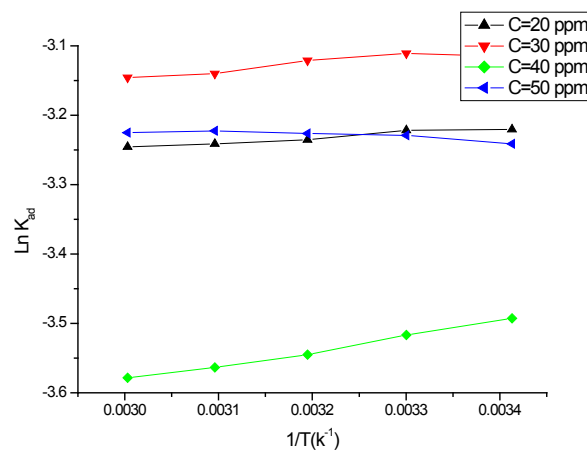


Fig. 14. Linearization curves of the distribution constant ($\ln K_0$) as a function of temperature ($1/T$) for Raw-Mag.

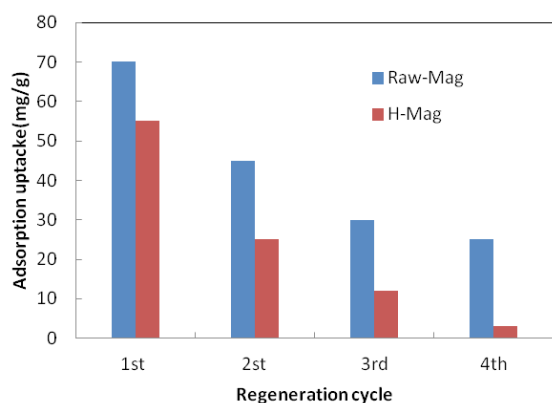


Fig. 15. Regeneration of Raw-Mag and Mag-H⁺ after adsorption of metribuzin ($V = 200$ mL, $M_1 = 0.1$ g, $M_2 = 0.04$ g, stirring speed = 250 rpm, and temperature = 20°C).

Table 8

Comparison of adsorption capacity of various adsorbents for metribuzin

Materials	q_m (mg/g)	Reference
Banana peel	166.66	[52]
Activated granular carbon	22	[13]
Corn Cob	4.07	[53]
Fly ash	0.56	[2]
Raw maghnite	70.1	This study
Acid-treated maghnite	55.6	This study

9. Conclusions

This study was carried out to investigate the use of system batch adsorption for the removal metribuzin from aqueous solution using raw maghnite and acid-activated maghnite. The sorption of metribuzin was dependent on the adsorbent dosage, stirring time, initial metribuzin concentration and pH solution. The both adsorbent used, raw-Mag and Mag-H⁺ have a surface area of 140 m²/g and 161 m²/g respectively. The adsorption experiments showed that metribuzin adsorption is more favorable at acidic medium. The maximum adsorption capacity was 70.1 and 55.6 mg/g for raw-Mag and Mag-H⁺ respectively, it was found at 20 mg/L initial concentration, and pH 2.5. The results showed that the pseudo-second order reaction kinetics model provided the best description of the adsorption. The experimental data for the adsorption process were well fitted by the Langmuir and Freundlich adsorption isotherm. Thermodynamic parameters were also evaluated for the system and revealed that the adsorption was endothermic in nature and spontaneous. Overall, the use of such as kind of materials is a double-win for both water treatment and soils.

References

- [1] S. Irace-Guigand, J.J. Aaron, P. Scribe, D. Barcelo, A comparison of the environmental impact of pesticide multiresidues and their occurrence in river waters surveyed by liquid chromatography coupled in tandem with UV diode array detection and mass spectrometry, *Chemosphere*, 55 (2004) 973–981.
- [2] N. Singh, Adsorption of herbicides on coal fly ash from aqueous solutions, *J. Hazard. Mater.*, 168 (2009) 233–237.
- [3] E. Ayranci, N. Hoda, Adsorption kinetics and isotherms of pesticides onto activated carbon-cloth, *Chemosphere*, 60 (2005) 1600–1607.
- [4] K. Majumdar, N. Singh, Effect of soil amendments on sorption and mobility of metribuzin in soils, *Chemosphere*, 66 (2007) 630–637.
- [5] O. Adam, P.M. Badot, F. Degiorgi, G. Crini, Mixture toxicity assessment of wood preservative pesticides in the freshwater amphipod *Gammarus pulex* (L.), *Ecotoxicol. Environ. Saf.*, 72 (2009) 441–449.
- [6] M.S. El-Geundi, T.E. Farrag, H.M.A. El-ghany, Adsorption equilibrium of a herbicide (pendimethalin) onto natural clay, *Adsorpt. Sci. Technol.*, 23 (2005) 437–453.
- [7] C. Moreno-Castilla, M.V. López-Ramón, L.M. Pastrana-Martínez, M.A. Álvarez-Merino, M.A. Fontecha-Cámara, Competitive adsorption of the herbicide fluroxypyr and tannic acid from distilled and tap water on activated carbons and their thermal desorption, *Adsorption*, 18 (2012) 173–179.
- [8] T. Reemtsma, The use of liquid chromatography-atmospheric pressure ionization-mass spectrometry in water analysis - Part I: Achievements, *Trends Anal.*, 20 (2001) 500–517.
- [9] M.Y. Hendawi, A.A. Romeh, T.M. Mekky, Effect of food processing on residue of imidacloprid in strawberry fruits, *J. Agric. Sci. Technol.*, 15 (2013) 951–959.
- [10] A. Liaghat, S.O. Prasher, Application of mathematical modeling to determine the size of on-site grass filters for reducing farm pesticide pollution, *Agric. Sci. Technol.*, 5 (2003).
- [11] C.R. Armendáriz, A.H. de la Torre, I.J.G. Fernández, G.L. González, Metribuzin, in: *Encycl. Toxicol.* Third Ed., 2014: pp. 327–329.
- [12] J. Skopalová, T. Navrátil, Application of elimination voltammetry to the study of electrochemical reduction and determination of the herbicide metribuzin, *Chem. Analyt. Chem.*, 52 (2007) 961–977.
- [13] O. Kitous, A. Cheikh, H. Lounici, H. Grib, A. Pauss, N. Mameri, Application of the electrosorption technique to remove metribuzin pesticide, *J. Hazard. Mater.*, 161 (2009) 1035–1039.
- [14] M. Antonopoulou, I. Konstantinou, Photocatalytic treatment of metribuzin herbicide over TiO₂ aqueous suspensions: removal efficiency, identification of transformation products, reaction pathways and ecotoxicity evaluation, *J. Photochem. Photobiol. A Chem.*, 294 (2014) 110–120.
- [15] O. Yahiaoui, L. Aizel, H. Lounici, N. Drouiche, M.F.A. Goosen, A. Pauss, N. Mameri, Evaluating removal of metribuzin pesticide from contaminated groundwater using an electrochemical reactor combined with ultraviolet oxidation, *Desalination*, 270 (2011) 84–89.
- [16] E. Ayranci, N. Hoda, Studies on removal of metribuzin, bromacil, 2,4-D and atrazine from water by adsorption on high area carbon cloth, *J. Hazard. Mater.*, 112 (2004) 163–168.
- [17] J.H. Yao, X. Li, W. Qin, Computational design and synthesis of molecular imprinted polymers with high selectivity for removal of aniline from contaminated water, *Anal. Chim. Acta.*, 610 (2008) 282–288.
- [18] D.C. Adams, L. Watson, Treatability of s-triazine herbicide metabolites using powdered activated carbon, *J. Environ. Eng. ASCE*, 39 (1996) 327–330.
- [19] J. Ludvík, P. Zuman, Adsorption of 1,2,4-triazine pesticides metamitron and metribuzin on lignin, *Microchem. J.*, 64 (2000) 15–20.
- [20] M.S. Fountoulakis, L. Makridis, E.K. Pirounaki, C. Chroni, A. Kyriacou, K. Lasaridi, T. Manios, Fate and effect of linuron and metribuzin on the co-composting of green waste and sewage sludge, *Waste Manage.*, 30 (2010) 41–49.
- [21] T.P.A. Shabeer, A. Saha, V.T. Gajbhiye, S. Gupta, K.M. Manjaiah, E. Varghese, Exploitation of nano-bentonite, nano-halloysite and organically modified nano-montmorillonite as an adsorbent and coagulation aid for the removal of multi-pesticides from water: A sorption modelling approach, *Water. Air. Soil Pollut.*, 226 (2015) 41.

- [22] A. Ourari, A. Flilissa, M. Boutahala, H. Iikiti, Removal of cetylpyridinium bromide by adsorption onto maghnite: Application to paper deinking, *J. Surfactants Deterg.*, 17 (2014) 785–793.
- [23] M.A. Zenasni, S. Benfarhi, A. Mansri, H. Benmehdi, B. Meroufel, J. Desbrieres, R. Dedriveres, Influence of pH on the uptake of toluene from water by the composite poly (4-vinylpyridinium)-maghnite, *African J. Pure Appl. Chem.*, 5 (2011) 486–493.
- [24] G. Fagerlund, Determination of specific surface by the BET method, *Matériaux Constr.*, 6 (1973) 239–245.
- [25] S. Brunauer, P.H. Emmett, E. Teller, Adsorption of gases in multimolecular layers, *J. Am. Chem. Soc.*, 60 (1938) 309–319.
- [26] A. Yahiaoui, M. Belbachir, A. Hachemaoui, An acid exchanged montmorillonite clay-catalyzed synthesis of polyepichlorhydrin, *Int. J. Mol. Sci.*, 4 (2003) 548–561.
- [27] N. Benharrats, M. Belbachir, A.P. Legrand, J.B. D’Espinoza de la Caillerie, 2 9Si and 2 7Al MAS NMR study of the zeolitization of kaolin by alkali leaching, *Clay Miner.*, 38 (2003) 49–61.
- [28] S. Zen, F.Z. El Berrichi, Adsorption of tannery anionic dyes by modified kaolin from aqueous solution, *Desal. Water Treat.*, 57 (2016) 6024–6032.
- [29] A. El-Kebir, A. Harrane, M. Belbachir, Protonated montmorillonite clay used as green non-toxic catalyst for the synthesis of biocompatible polyglycidol, *Arab. J. Sci. Eng.*, 41 (2016) 2179–2184.
- [30] J. Madejová, FTIR techniques in clay mineral studies, *Vib. Spectrosc.*, 31 (2003) 1–10.
- [31] P. Komadel, Chemically modified smectites, *Clay Miner.*, 38 (2003) 127–138.
- [32] F.Z. Zeggai, A. Hachemaoui, A. Yahiaoui, Chemical synthesis of nanocomposites via intercalative polymerisation of 4-aminobenzyl amine and aniline using exchanged montmorillonite, *J. Mater. Environ. Sci.*, 6 (2015) 2315–2321.
- [33] D. Prodanović, Ž.D. Živković, M. Dumić, The kinetics of dehydroxylation and mullitization of zettlitz kaolin in the presence of calcium(II) as an ingredient, *Thermochim. Acta.*, 156 (1989) 61–67.
- [34] X. Ren, Z. Zhang, H. Luo, B. Hu, Z. Dang, C. Yang, L. Li, Adsorption of arsenic on modified montmorillonite, *Appl. Clay Sci.*, 97–98 (2014) 17–23.
- [35] B. Ma, S. Oh, W.S. Shin, S.J. Choi, Removal of Co^{2+} , Sr^{2+} and Cs^+ from aqueous solution by phosphate-modified montmorillonite (PMM), *Desalination*, 276 (2011) 336–346.
- [36] J.P. Chen, S.O. Pehkonen, C.C. Lau, Phorate and Terbufos adsorption onto four tropical soils, *Colloids Surfaces A Physicochem. Eng. Asp.*, 240 (2004) 55–61.
- [37] R. Celis, C. Trigo, G. Facenda, M.D.C. Hermosín, J. Cornejo, Selective modification of clay minerals for the adsorption of herbicides widely used in olive groves, *J. Agric. Food Chem.*, 55 (2007) 6650–6658.
- [38] M. Mekhloufi, A. Zehhaf, A. Benyoucef, C. Quijada, E. Morallon, Removal of 8-quinolinecarboxylic acid pesticide from aqueous solution by adsorption on activated montmorillonites, *Environ. Monit. Assess.*, 185 (2013) 10365–10375.
- [39] D. Lozano-Castelló, F. Suárez-García, D. Cazorla-Amorós, Á. Linares-Solano, Porous texture of carbons, in: *Carbons Electrochem. Energy Storage Convers. Syst.*, 2009: pp. 115–162.
- [40] T.S. Anirudhan, P.S. Suchithra, S. Rijith, Amine-modified polyacrylamide-bentonite composite for the adsorption of humic acid in aqueous solutions, *Colloids Surfaces A Physicochem. Eng. Asp.*, 326 (2008) 147–156.
- [41] A. Marsal, E. Bautista, I. Ribosa, R. Pons, M.T. García, Adsorption of polyphenols in wastewater by organo-bentonites, *Appl. Clay Sci.*, 44 (2009) 151–155.
- [42] L. Lei, X. Li, X. Zhang, Ammonium removal from aqueous solutions using microwave-treated natural Chinese zeolite, *Sep. Purif. Technol.*, 58 (2008) 359–366.
- [43] B.V. Babu, S. Gupta, Adsorption of Cr(VI) using activated neem leaves: Kinetic studies, *Adsorption*, 14 (2008) 85–92.
- [44] S. Sen Gupta, K.G. Bhattacharyya, Immobilization of Pb(II), Cd(II) and Ni(II) ions on kaolinite and montmorillonite surfaces from aqueous medium, *J. Environ. Manage.*, 87 (2008) 46–58.
- [45] K.Y. Foo, B.H. Hameed, Insights into the modeling of adsorption isotherm systems, *Chem. Eng. J.*, 156 (2010) 2–10.
- [46] T.X. Bui, H. Choi, Adsorptive removal of selected pharmaceuticals by mesoporous silica SBA-15, *J. Hazard. Mater.*, 168 (2009) 602–608.
- [47] N. Gupta, A.K. Kushwaha, M.C. Chattopadhyaya, Adsorptive removal of Pb^{2+} , Co^{2+} and Ni^{2+} by hydroxyapatite/chitosan composite from aqueous solution, *J. Taiwan Inst. Chem. Eng.*, 43 (2012) 125.
- [48] Y. Ho, G. McKay, Pseudo-second order model for sorption processes, *Process Biochem.*, 34 (1999) 451–465.
- [49] M.F. Brigatti, C. Lugli, L. Poppi, Kinetics of heavy-metal removal and recovery in sepiolite, in: *Appl. Clay Sci.*, 2000: pp. 45–57.
- [50] A.M. Donia, A.A. Atia, H. El-Boraey, D.H. Mabrouk, Uptake studies of copper(II) on glycidyl methacrylate chelating resin containing Fe_3O_3 particles, *Sep. Purif. Technol.*, 49 (2006) 64–70.
- [51] H.M.F. Freundlich, Über Die Absorption in Lösungen, *Z. Phys. Chem.*, 57 (1906) 385–470.
- [52] A. ul Haq, J. Shah, M.R. Jan, S. ud Din, Kinetic, equilibrium and thermodynamic studies for the sorption of metribuzin from aqueous solution using banana peels, an agro-based biomass, *Toxicol. Environ. Chem.*, 97 (2015) 124–134.
- [53] B. Ara, J. Shah, M.R. Jan, S. Aslam, Removal of metribuzin herbicide from aqueous solution using corn cob, *Int. J. Sci. Environ.*, 2 (2013) 146–161.